

## Stimulated Rayleigh Scattering Enhanced by a Longitudinal Plasma Mode in a Periodically Driven Dirac Semimetal $\text{Cd}_3\text{As}_2$

Yuta Murotani<sup>1,\*</sup>, Natsuki Kanda<sup>1,2,\*</sup>, Tatsuhiko N. Ikeda<sup>1</sup>, Takuya Matsuda<sup>1</sup>, Manik Goyal<sup>3</sup>, Jun Yoshinobu<sup>1</sup>, Yohei Kobayashi<sup>1</sup>, Susanne Stemmer<sup>3</sup>, and Ryusuke Matsunaga<sup>1,2,§</sup>

<sup>1</sup>The Institute for Solid State Physics, The University of Tokyo, Kashiwa, Chiba 277-8581, Japan

<sup>2</sup>PRESTO, Japan Science and Technology Agency, 4-1-8 Honcho Kawaguchi, Saitama 332-0012, Japan

<sup>3</sup>Materials Department, University of California, Santa Barbara, California 93106-5050, USA

 (Received 5 May 2022; revised 6 July 2022; accepted 17 October 2022; published 10 November 2022)

Using broadband (12–45 THz) multi-terahertz spectroscopy, we show that stimulated Rayleigh scattering dominates the transient optical conductivity of cadmium arsenide, a Dirac semimetal, under an optical driving field at 30 THz. The characteristic dispersive line shape with net optical gain is accounted for by optical transitions between light-induced Floquet subbands, strikingly enhanced by the longitudinal plasma mode. Stimulated Rayleigh scattering with an unprecedentedly large refractive index change may pave the way for slow light generation in conductive solids at room temperature.

DOI: [10.1103/PhysRevLett.129.207402](https://doi.org/10.1103/PhysRevLett.129.207402)

Light has opened various ways to reach interesting nonequilibrium phases of matter, such as light-induced superconductivity [1,2], charge density wave [3], and excitonic insulator [4]. The emerging field of Floquet engineering is accelerating new discoveries through the versatility of periodic driving to modify material properties [5,6]. Examples include control of band topology [7–10] and of excitonic correlations [11,12]. Floquet engineering is also interesting from the viewpoint of nonlinear optics. Historically, the concept of photon-dressed states has provided an indispensable basis to understand the nonlinear optical response of discrete level systems [13]. Modern interest in Floquet engineering has extended the idea of dressed states to continuous bands in solids, revealing new aspects of nonlinear optics, e.g., in terms of topology [14]. It is thus natural to expect novel optical phenomena to emerge from light-induced Floquet states.

Despite remarkable progress in theory, experimental exploration of Floquet states is still limited. Time- and angle-resolved photoemission spectroscopy succeeded in directly observing electron population in photon-dressed Floquet-Bloch bands on a surface of a light-driven topological insulator [15,16]. Ultrafast transport measurement has recently demonstrated that irradiation by circularly polarized light transforms graphene into a Floquet topological insulator [7,17], which partly contributes to the anomalous Hall effect [18]. Manifestations of the light-induced Floquet states in the optical response itself, however, remain unclear. Little has been known about fundamental optical properties of Floquet states in solids, except for the well-known ac Stark effect of discrete levels. Cadmium arsenide ( $\text{Cd}_3\text{As}_2$ ), a three-dimensional Dirac semimetal, is an ideal material to investigate this problem, because it combines high-mobility carriers, a small

scattering rate, and low-energy interband transitions [19], which allow for coherent dynamics with suppressed dissipation and laser heating. Moreover,  $\text{Cd}_3\text{As}_2$  exhibits large optical nonlinearity in a broad frequency region ranging from terahertz to visible [20–25], which makes it a promising platform to search for novel functionality in nonlinear optics and optoelectronics from the perspective of Floquet engineering.

Figure 1(a) shows the band structure of  $\text{Cd}_3\text{As}_2$ . Two Dirac nodes lie on the  $k_z$  axis, which allow low-energy interband transitions [19,26]. The valence and conduction bands are expected to form Floquet states upon periodic driving by a light field, as shown in Fig. 1(b). To explore the spectroscopic signature and optical functionality of the Floquet states, we measure transient optical conductivity of an epitaxially grown, (112)-oriented, 140 nm-thick  $\text{Cd}_3\text{As}_2$  thin film on a CdTe substrate [27], exposed to an intense multi-terahertz electromagnetic pulse at room temperature. Figure 1(c) depicts the experimental setup. Our sample is unintentionally electron-doped so that the Fermi level is shifted to 58 meV above the Dirac nodes [25]. Despite the anisotropy in the low-energy band structure, the linear response in the infrared region is almost isotropic because of the quasi-cubic nature of the structural units that make up the unit cell [36,37]. Figure 1(d) shows the optical conductivity of the sample in equilibrium. It can be decomposed into the low-frequency (<15 THz) intraband and high-frequency (>15 THz) interband contributions, by taking account of the low-frequency data outside the panel [25,38]. The narrowband pump pulse drives the interband transitions with a tunable frequency from 16 to 40 THz (66–165 meV in energy, 8–19  $\mu\text{m}$  in wavelength) and with a variable bandwidth, while the probe pulse covers a broad frequency range from 12 to 45 THz (50–186 meV,

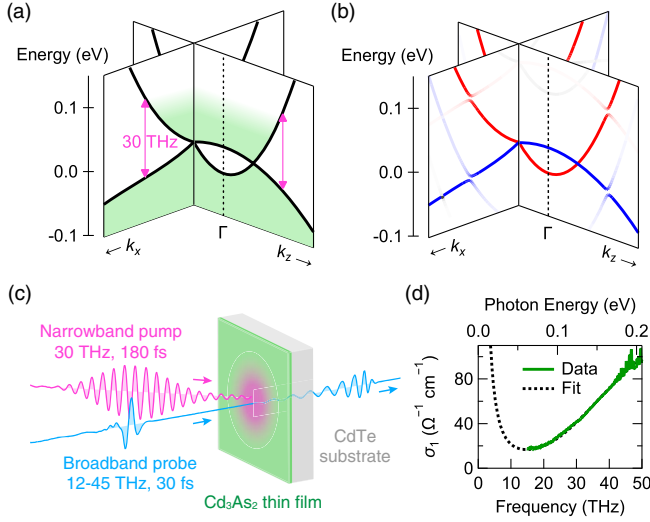


FIG. 1. (a) Band structure of  $\text{Cd}_3\text{As}_2$  around the  $\Gamma$  point [26]. (b) Schematic picture of the Floquet state formation by a periodic optical field. (c) Setup of the pump-probe experiment. (d) Optical conductivity of the sample. The model fitting (dotted line) takes into account the lower-frequency data outside the panel [25].

7–25  $\mu\text{m}$ ) with a duration of 30 fs. The probe pulse after transmitting the sample is spatially separated from the pump pulse and is detected by electro-optic sampling to obtain response functions depending on the pump-probe delay time  $\Delta t$  [27].

Figure 2(a) shows the transient optical conductivity measured by probe pulses polarized in the same direction as the pump, tuned to 29.4 THz. During the pump irradiation, a photoinduced absorption (blue) appears just below the pump frequency, while an opposite change (red) occurs on the higher-frequency side. The resulting dispersive line shape is clearly seen in Fig. 2(b), which plots the optical conductivity at several delay times. This characteristic behavior is distinct both from spectral hole burning [39] and from photon-assisted absorption bands [40], the two scenarios that have been theoretically considered so far. Note that net optical gain ( $\sigma_1 < 0$ ) develops from the suppressed absorption at around the maximum pump-probe overlap ( $\Delta t \simeq 0$  ps). The dispersive structure vanishes after the pump pulse leaves the sample, as visualized in Fig. 2(d). Upon changing the pump fluence, positions of the peak and the dip stay almost constant, as shown in Fig. 2(e). We also plot in the same figure the fluence dependence of the peak and dip values along with the equilibrium values at 28.2 and 31.3 THz (open triangles). In the weak excitation limit ( $< 0.1 \text{ mJ/cm}^2$ ), both the peak and the dip grow linearly with the pump fluence, indicating a perturbative origin of the signal. We found that no dispersive signal appears when the probe is polarized perpendicularly to the pump [27], implying a coherent nature of the involved processes. In addition, Fig. 2(c) verifies that the position of the dispersive structure

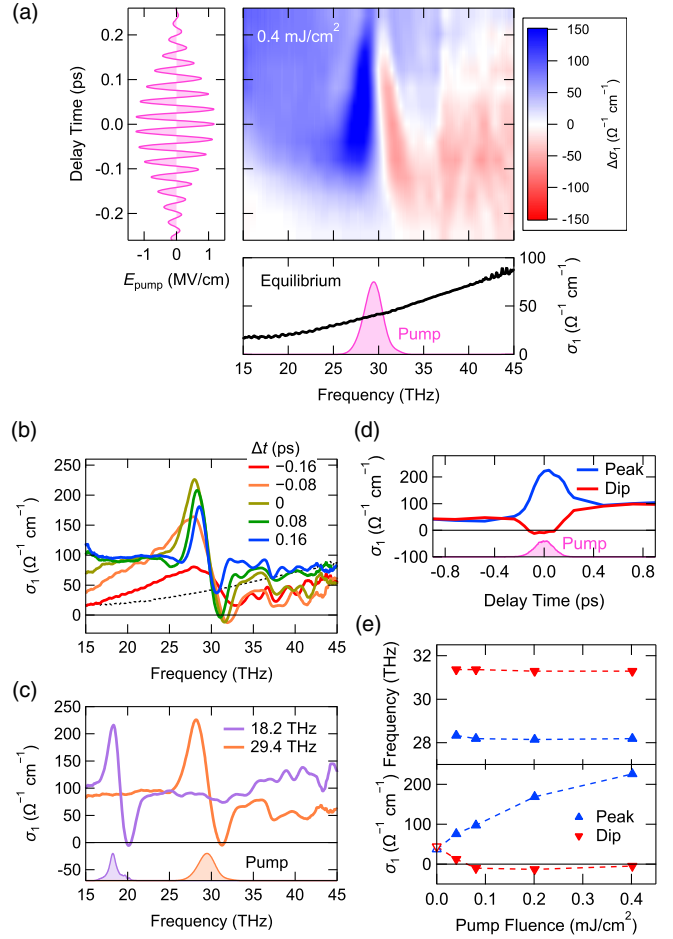


FIG. 2. (a) Change of the optical conductivity as a function of frequency (horizontal axis) and pump-probe delay time  $\Delta t$  (vertical axis). Waveform of the pump pulse is shown on the left. The equilibrium optical conductivity is plotted on the bottom along with the pump power spectrum. Pump and probe pulses are collinearly polarized. (b) Transient optical conductivity at several delay times. The equilibrium spectrum is shown as a dotted line. (c) Optical conductivity at  $\Delta t = 0.04$  ps for different pump frequencies, i.e., 29.4 [the same as in (a),(b)] and 18.2 THz (with a fluence of  $0.25 \text{ mJ/cm}^2$ , a peak electric field of  $0.9 \text{ MV/cm}$ ). (d) Delay time dependence of the peak and dip values extracted from (a). Temporal profile of the pump intensity is shown as the shaded curve. (e) Top: Positions of the peak and the dip in optical conductivity at  $\Delta t = 0.04$  ps, as a function of pump fluence. Bottom: A similar plot for the conductivity values at the peak and the dip. Equilibrium values at 28.2 and 31.3 THz are added as open triangles.

follows the center frequency of the pump, excluding the possibility that the signal could arise from some special points in the band structure or specific phonon modes.

In the case of semiconductors, it is known that a dispersive absorption change appears in the early stage of photoexcitation as a result of excitonic effect [41,42]. In this mechanism, however, the absorption peak should lie on the higher energy side of the pump photon energy, which is

opposite to the behavior observed here. Thus, excitonic effects are of minor importance in  $\text{Cd}_3\text{As}_2$ , consistent with recent predictions [43].

From a phenomenological point of view, the dispersive absorption change in  $\text{Cd}_3\text{As}_2$  can be understood in terms of stimulated Rayleigh scattering (SRLS). Suppose that application of the optical field primarily changes the real part of the refractive index. When the pump and probe beams spatially overlap, their interference creates a transient grating, which diffracts the pump beam into two directions; one is a new direction often studied in four-wave mixing experiments, and the other the propagation direction of the probe, as shown in Fig. 3(e). The latter effect suppresses or enhances absorption of the probe beam depending on the phase of the diffracted wave. In case of a negative refractive index change, this process results in a photoinduced absorption (emission) for a probe frequency slightly lower (higher) than the pump, as seen in Fig. 3(a). This mechanism accounts for our experimental results, because

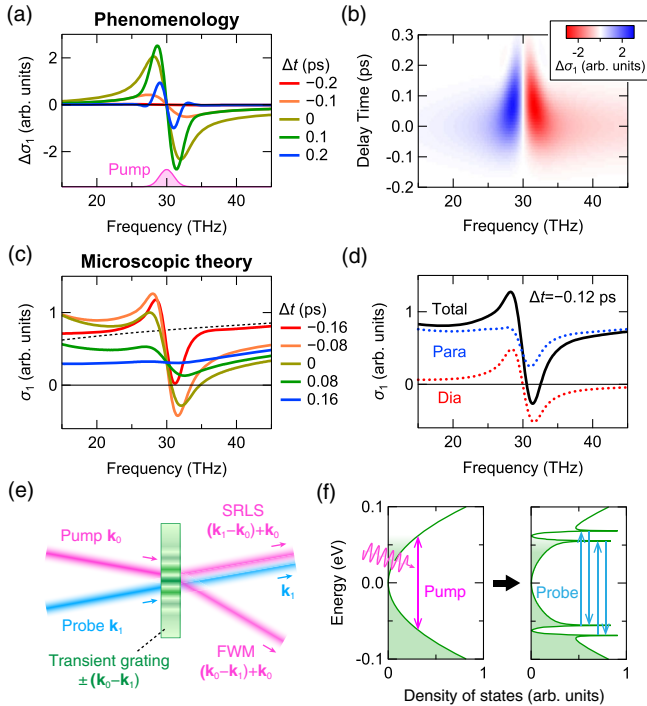


FIG. 3. (a) Change of the optical conductivity  $\Delta\sigma_1$  calculated by a phenomenological model. Theoretical details are given in Supplemental Material [27]. (b) Two-dimensional plot of  $\Delta\sigma_1$  as a function of frequency (horizontal axis) and pump-probe delay time (vertical axis). (c) Transient optical conductivity calculated by a microscopic model. (d) Contributions from the paramagnetic (blue) and diamagnetic (red) currents in the total optical conductivity (black) at  $\Delta t = -0.12$  ps. (e) Geometric picture of stimulated Rayleigh scattering (SRLS) and four-wave mixing (FWM).  $\mathbf{k}_0$  and  $\mathbf{k}_1$  denote wave vectors of the pump and the probe, respectively. (f) SRLS induced by Floquet states in continuous bands. Ordinary ac Stark effect corresponds to transitions between the topmost and bottom peaks, and between the intermediate peaks, in the right panel.

interband excitation actually reduces the refractive index through a blueshift of the longitudinal plasma mode initially located at 10 THz [25,27]. The blueshift is associated with increased density of charge carriers, since the squared plasma frequency is proportional to the carrier density. In nonlinear optics, light scattering by light-induced density fluctuations of gases and crystals is known as SRLS [13]. Therefore, the process described above also belongs to SRLS, which utilizes the collective plasma oscillation of charge carriers as a novel source of it. We note that this mechanism of SRLS is distinct from the conventional ones not only qualitatively—in its origin—but also quantitatively. The collective nature of the plasma mode enables a large refractive index change more than 1 [27], which far exceeds the known cases and thus leads to unprecedentedly strong SRLS. It is interesting that metallic response of solids with the plasma mode significantly enhances the coherent light-matter interaction. We will discuss a possible application of such a large refractive index change later. In the phenomenological model presented above, the separation between the peak and the dip decreases for increasing  $\Delta t$  as shown in Fig. 3(b), consistent with the experimental result in Fig. 2(a). Such a narrowing is explained by the detection scheme in our experiment [27].

We next consider the quantum mechanical aspect of this phenomenon and discuss its connection to the Floquet states. In Fig. 3(c), we plot the transient optical conductivity calculated by an effective two-band model for the low-energy band structure [27]. One can clearly recognize a dispersive line shape. Knowledge of two-level systems helps us to interpret this result using a level diagram. In two-level systems, the well-known ac Stark effect is accompanied by a dispersive structure at the pump frequency, also called SRLS [13,27]. It originates from transitions between dressed states in resonance with the driving field. Extending this understanding to the continuous bands, SRLS in  $\text{Cd}_3\text{As}_2$  is attributed to transitions between the Floquet subbands resonant to the pump frequency, as schematically shown in Fig. 3(f). Relatively small scattering rates in  $\text{Cd}_3\text{As}_2$  justify such a Floquet state picture. A closer look at its origin, however, reveals the difference of light-matter interaction responsible for SRLS in  $\text{Cd}_3\text{As}_2$  and in two-level systems. In the latter, a usual coupling between electric dipole moments and the electric field, also called paramagnetic coupling, induces relatively weak SRLS, with a sign depending on detuning [13]. As a result, SRLS in two-level systems tends to be canceled out when integrated over continuous bands, leaving a spectral hole stemming from the ac Stark effect and Pauli blocking [39]. This consequence can be seen in the blue curve in Fig. 3(d), which plots the contribution from the paramagnetic coupling only. The dispersive structure in the total optical conductivity arises from a second-order or diamagnetic coupling with the electric field, which yields the red curve in Fig. 3(d) showing good agreement with the

experimental result. This coupling causes a light-induced shift of the screened plasma frequency, so that the microscopic theory also supports the phenomenological picture presented above. In Supplemental Material, we derive the macroscopic model by analyzing the diamagnetic current in the microscopic model [27]. The derivation tells us that an intermediate frequency between intraband and interband transitions is preferable, because SRLS in this case requires a combination of injection and acceleration of photocarriers. These findings renew the prospect of Floquet engineering for optical properties of matter, because the importance of the diamagnetic coupling has not been recognized so far. Since the above discussion does not rely on details of the band structure, SRLS is expected to occur in general semimetals and narrow-gap semiconductors with low-energy interband transitions.

Finally, from a perspective of Floquet engineering of optical functionality, we discuss the possibility of slow light generation in  $\text{Cd}_3\text{As}_2$ . Consistent with a general property of SRLS [13], the dispersive structure in transient optical conductivity can be narrowed by reducing the pump bandwidth, as shown in Fig. 4(a). Such a narrow structure in absorption is necessarily accompanied with a rapid variation in the refractive index  $n$  with frequency  $f$ , so that the group refractive index  $n_g = n + f(dn/df)$  may become large. The resultant slowing down of an optical wave packet is known as slow light generation [13,44–50]. In the present experiment, we directly evaluate the broadband refractive index as a complex quantity. The top panel in Fig. 4(b) shows that a narrow dip in the refractive index develops at, e.g.,  $\Delta t = -0.48$  ps, leading to a group refractive index as large as 40 at 30 THz [bottom panel in Fig. 4(b)]. This corresponds to 40 times deceleration of a wave packet, free from dissipation because of the negative extinction coefficient  $\kappa$  [middle panel in Fig. 4(b)]. An even more interesting situation occurs when a metallic screening ( $\epsilon_1 < 0$ ) by photoexcited carriers coexists with an optical gain ( $\epsilon_2 < 0$ ), where  $\epsilon_1$  and  $\epsilon_2$  stand for the real and imaginary parts of the dielectric constant, respectively. The refractive index  $n = [(\sqrt{\epsilon_1^2 + \epsilon_2^2} + \epsilon_1)/2]^{1/2}$  then vanishes at the boundary between absorption and gain ( $\epsilon_2 = 0$ ), which may further enhance the rapid spectral variation in  $n$  [top panel in Fig. 4(c)]. The group index correspondingly exceeds 300 at  $\Delta t = -0.24$  ps [bottom panel in Fig. 4(d)], where a metallic screening ( $\epsilon_1 < 0$ ) develops with the help of the SRLS itself. Remarkably, the extinction coefficient  $\kappa = (\text{sgn}\epsilon_2)[(\sqrt{\epsilon_1^2 + \epsilon_2^2} - \epsilon_1)/2]^{1/2}$  remains negative in this gain region [middle panel in Fig. 4(c)], so that a probe wave does not decay in spite of the metallic character in  $\epsilon_1$ . An electromagnetic pulse therefore might be slowed down more than 300 times without loss under the present experimental condition.

Most previous studies of slow light generation used electromagnetically induced transparency [44–46,49] and photonic-band engineering [50] as the origin of a refractive index change  $\Delta n$ , which typically amounts to  $\sim 0.01$  and

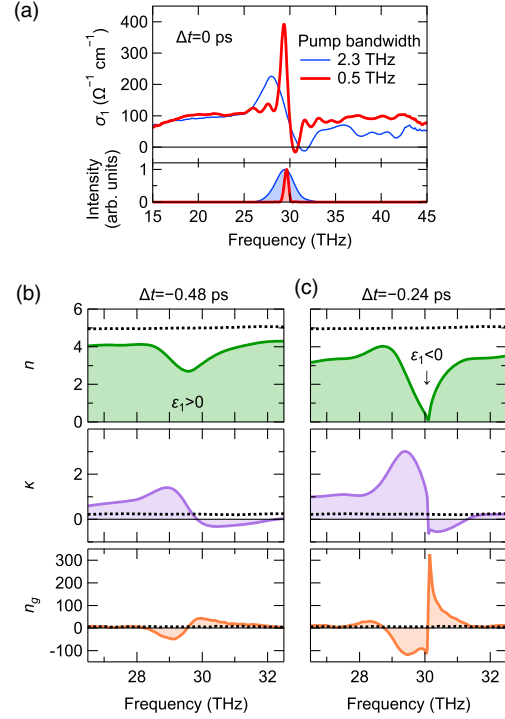


FIG. 4. (a) Transient optical conductivity for broader (thin) and narrower (thick) pump pulses. Pump power spectra are plotted on the bottom with their FWHM indicated in the figure. The broader pump is the same as in Fig. 2(a), while the narrower one has a pulse width of 0.88 ps, a fluence of 1.7 mJ/cm<sup>2</sup>, and a peak electric field of 1.2 MV/cm. (b) Refractive index  $n$  (top), extinction coefficient  $\kappa$  (middle), and group refractive index  $n_g$  (bottom) measured at  $\Delta t = -0.48$  ps for the narrower pump in (a). Equilibrium spectra are shown as dotted lines. (c) The same dataset for  $\Delta t = -0.24$  ps.

$\sim 0.1$ , respectively. In our case, by contrast,  $\Delta n > 1$  is so large that  $n$  even vanishes. A relatively large bandwidth  $\Delta f \sim 0.5$  THz of the dispersion limits the achievable group refractive index here. This is not necessarily a disadvantage, because a broader dispersion allows a shorter pulse to be slowed down. In fact, photonic-band engineering emerged as a way to generate slow light with a broad bandwidth ( $\sim$ THz) [50], compared to a much narrower one ( $\sim$ kHz) achieved by electromagnetically induced transparency. Our experimental results show that lossless and broadband slow light generation is possible by simply shedding infrared light to a semimetal at room temperature. To avoid complication by transient effects, such as the temporal change from Figs. 4(b) to 4(c), continuous-wave or nanosecond  $\text{CO}_2$  lasers promise better choice as the pump light source, though optical heating should be suppressed by efficient cooling. We expect SRLS to be robust against excitation-induced dephasing and scattering even for such a long-lasting driving, because its coherence time is determined by the relatively long carrier lifetime  $T_1 = 8$  ps. The available bandwidth then becomes  $\Delta f \sim 1/T_1 = 0.13$  THz, still keeping a relatively large

value. We leave the implementation of slow light generation with this mechanism as a topic of future studies.

In summary, we performed ultrafast pump-probe spectroscopy on a  $\text{Cd}_3\text{As}_2$  thin film in the multi-terahertz frequency region, to find SRLS to dominate the transient absorption spectrum in the pump-probe overlap. Macroscopically, it originates from a transient grating with a blueshifted plasma frequency in the interfering pump and probe fields. The characteristic dispersive line shape can be further traced back to microscopic optical transitions between the light-dressed electronic bands, the Floquet subbands, assisted by a diamagnetic coupling with the optical field. The concomitant sharp dispersion in the transient refractive index may be applicable to semi-metal-based, lossless, broadband slow light generation at room temperature. These findings reveal a general aspect of light-matter interaction and lay the foundation of Floquet engineering for optical response of continuous energy bands. The application of circularly polarized driving fields promises an interesting future direction because of its ability to manipulate band topology and magnetic symmetry [8–10,51,52].

This work was supported by JST PRESTO (Grants No. JPMJPR20LA and No. JPMJPR2006), JST CREST (Grant No. JPMJCR20R4), and in part by JSPS KAKENHI (Grants No. JP19H01817 and No. JP20J01422, No. JP20H00343, and No. JP21K13852). Work at UCSB was supported by CATS Energy Frontier Research Center, which is funded by the U.S. Department of Energy, Basic Energy Sciences, under Contract No. DE-AC02-06CH11357. R. M. also acknowledges partial support by Attosecond lasers for next frontiers in science and technology (ATTO) in Quantum Leap Flagship Program (MEXT Q-LEAP). A part of the computations and the FTIR measurement were performed using the facilities of the Supercomputer Center and the Materials Design and Characterization Laboratory, respectively, in The Institute for Solid State Physics, The University of Tokyo. R. M. conceived this project. M. G. and S. S. fabricated the sample. N. K. and T. M. evaluated the linear response function. Y. M. and N. K. developed the pump-probe spectroscopy system with the help of J. Y., Y. K., and R. M. N. K. performed the experiment and analyzed the data. Y. M. conducted the phenomenological analysis. Y. M. and T. N. I. performed the microscopic calculations. All the authors discussed the results. Y. M. wrote the manuscript with the substantial help of N. K., T. N. I., and R. M., with the feedbacks from all the other coauthors.

\*These authors contributed equally to this work.

†murotani@issp.u-tokyo.ac.jp

‡n-kanda@issp.u-tokyo.ac.jp

§matsunaga@issp.u-tokyo.ac.jp

- [1] M. Mitrano *et al.*, Possible light-induced superconductivity in  $\text{K}_3\text{C}_{60}$  at high temperature, *Nature (London)* **530**, 461 (2016).
- [2] M. Budden *et al.*, Evidence for metastable photo-induced superconductivity in  $\text{K}_3\text{C}_{60}$ , *Nat. Phys.* **17**, 611 (2021).
- [3] A. Kogar *et al.*, Light-induced charge density wave in  $\text{LaTe}_3$ , *Nat. Phys.* **16**, 159 (2020).
- [4] Y. Murotani, C. Kim, H. Akiyama, L. N. Pfeiffer, K. W. West, and R. Shimano, Light-Driven Electron-Hole Bardeen-Cooper-Schrieffer-Like State in Bulk GaAs, *Phys. Rev. Lett.* **123**, 197401 (2019).
- [5] T. Oka and S. Kitamura, Floquet engineering of quantum materials, *Annu. Rev. Condens. Matter Phys.* **10**, 387 (2019).
- [6] U. De Giovannini and H. Hübener, Floquet analysis of excitations in materials, *J. Phys. Mater.* **3**, 012001 (2020).
- [7] T. Oka and H. Aoki, Photovoltaic Hall effect in graphene, *Phys. Rev. B* **79**, 081406(R) (2009).
- [8] R. Wang, B. Wang, R. Shen, L. Sheng, and D. Y. Xing, Floquet Weyl semimetal induced by off-resonant light, *Europhys. Lett.* **105**, 17004 (2014).
- [9] S. Ebihara, K. Fukushima, and T. Oka, Chiral pumping effect induced by rotating electric fields, *Phys. Rev. B* **93**, 155107 (2016).
- [10] H. Hübener, M. A. Sentef, U. De Giovannini, A. F. Kemper, and A. Rubio, Creating stable Floquet–Weyl semimetals by laser-driving of 3D Dirac materials, *Nat. Commun.* **8**, 13940 (2017).
- [11] E. Perfetto, D. Sangalli, A. Marini, and G. Stefanucci, Pump-driven normal-to-excitonic insulator transition: Josephson oscillations and signatures of BEC-BCS crossover in time-resolved ARPES, *Phys. Rev. Mater.* **3**, 124601 (2019).
- [12] E. Perfetto and G. Stefanucci, Floquet Topological Phase of Nondriven p-Wave Nonequilibrium Excitonic Insulators, *Phys. Rev. Lett.* **125**, 106401 (2020).
- [13] R. W. Boyd, *Nonlinear Optics*, 4th ed. (Academic Press, Cambridge, 2020).
- [14] T. Morimoto and N. Nagaosa, Topological nature of nonlinear optical effects in solids, *Sci. Adv.* **2**, e1501524 (2016).
- [15] Y. H. Wang, H. Steinberg, P. Jarillo-Herrero, and N. Gedik, Observation of Floquet-Bloch states on the surface of a topological insulator, *Science* **342**, 453 (2013).
- [16] F. Mahmood, C.-K. Chan, Z. Alpichshev, D. Gardner, Y. Lee, P. A. Lee, and N. Gedik, Selective scattering between Floquet–Bloch and Volkov states in a topological insulator, *Nat. Phys.* **12**, 306 (2016).
- [17] J. W. McIver, B. Schulte, F.-U. Stein, T. Matsuyama, G. Jotzu, G. Meier, and A. Cavalleri, Light-induced anomalous Hall effect in graphene, *Nat. Phys.* **16**, 38 (2020).
- [18] S. A. Sato *et al.*, Microscopic theory for the light-induced anomalous Hall effect in graphene, *Phys. Rev. B* **99**, 214302 (2019).
- [19] I. Crassee, R. Sankar, W.-L. Lee, A. Akrap, and M. Orlita, 3D Dirac semimetal  $\text{Cd}_3\text{As}_2$ : A review of material properties, *Phys. Rev. Mater.* **2**, 120302 (2018).
- [20] Q. Wang *et al.*, Ultrafast broadband photodetectors based on three-dimensional Dirac semimetal  $\text{Cd}_3\text{As}_2$ , *Nano Lett.* **17**, 834 (2017).

- [21] C. Zhu *et al.*, A robust and tuneable mid-infrared optical switch enabled by bulk Dirac fermions, *Nat. Commun.* **8**, 14111 (2017).
- [22] B. Cheng, N. Kanda, T.N. Ikeda, T. Matsuda, P. Xia, T. Schumann, S. Stemmer, J. Itatani, N.P. Armitage, and R. Matsunaga, Efficient Terahertz Harmonic Generation with Coherent Acceleration of Electrons in the Dirac Semimetal  $\text{Cd}_3\text{As}_2$ , *Phys. Rev. Lett.* **124**, 117402 (2020).
- [23] S. Kovalev *et al.*, Non-perturbative terahertz high-harmonic generation in the three-dimensional Dirac semimetal  $\text{Cd}_3\text{As}_2$ , *Nat. Commun.* **11**, 2451 (2020).
- [24] J. Lim, Y.S. Ang, F.J. García de Abajo, I. Kaminer, L.K. Ang, and L.J. Wong, Efficient generation of extreme terahertz harmonics in three-dimensional Dirac semimetals, *Phys. Rev. Res.* **2**, 043252 (2020).
- [25] N. Kanda, Y. Murotani, T. Matsuda, M. Goyal, S. Salmani-Rezaie, J. Yoshinobu, S. Stemmer, and R. Matsunaga, Tracking ultrafast change of multiterahertz broadband response functions in a photoexcited Dirac semimetal  $\text{Cd}_3\text{As}_2$  thin film, *Nano Lett.* **22**, 2358 (2022).
- [26] Z. Wang, H. Weng, Q. Wu, X. Dai, and Z. Fang, Three-dimensional Dirac semimetal and quantum transport in  $\text{Cd}_3\text{As}_2$ , *Phys. Rev. B* **88**, 125427 (2013).
- [27] See Supplemental Material at <http://link.aps.org/supplemental/10.1103/PhysRevLett.129.207402>, which includes Refs. [28–35], for the experimental methods, additional analysis, and details of theoretical consideration.
- [28] M. Goyal, L. Galletti, S. Salmani-Rezaie, T. Schumann, D. A. Kealhofer, and S. Stemmer, Thickness dependence of the quantum Hall effect in films of the three-dimensional Dirac semimetal  $\text{Cd}_3\text{As}_2$ , *APL Mater.* **6**, 026105 (2018).
- [29] A. Sell, A. Leitenstorfer, and R. Huber, Phase-locked generation and field-resolved detection of widely tunable terahertz pulses with amplitudes exceeding 100 MV/cm, *Opt. Lett.* **33**, 2767 (2008).
- [30] B. Liu, H. Bromberger, A. Cartella, T. Gebert, M. Först, and A. Cavalleri, Generation of narrowband, high-intensity, carrier-envelope phase-stable pulses tunable between 4 and 18 THz, *Opt. Lett.* **42**, 129–131 (2017).
- [31] C.-H. Lu, Y.-J. Tsou, H.-Y. Chen, B.-H. Chen, Y.-C. Cheng, S.-D. Yang, M.-C. Chen, C.-C. Hsu, and A.H. Kung, Generation of intense supercontinuum in condensed media, *Optica* **1**, 400 (2014).
- [32] N. Kanda, N. Ishii, J. Itatani, and R. Matsunaga, Optical parametric amplification of phase-stable terahertz-to-mid-infrared pulses studied in the time domain, *Opt. Exp.* **29**, 3479 (2021).
- [33] J. T. Kindt and C. A. Schmuttenmaer, Theory for determination of the low-frequency time-dependent response function in liquids using time-resolved terahertz pulse spectroscopy, *J. Chem. Phys.* **110**, 8589 (1999).
- [34] J. Orenstein and J. S. Dodge, Terahertz time-domain spectroscopy of transient metallic and superconducting states, *Phys. Rev. B* **92**, 134507 (2015).
- [35] Q. T. Vu and H. Haug, Detection of light-induced band gaps by ultrafast femtosecond pump and probe spectroscopy, *Phys. Rev. B* **71**, 035305 (2005).
- [36] A. Akrap, M. Haki, S. Tchoumakov, I. Crassee, J. Kuba *et al.*, Magneto-Optical Signature of Massless Kane Electrons in  $\text{Cd}_3\text{As}_2$ , *Phys. Rev. Lett.* **117**, 136401 (2016).
- [37] A. Mosca Conte, O. Pulci, and F. Bechstedt, Electronic and optical properties of topological semimetal  $\text{Cd}_3\text{As}_2$ , *Sci. Rep.* **7**, 45500 (2017).
- [38] D. Neubauer, J. P. Carbotte, A. A. Nateprov, A. Löhle, M. Dressel, and A. V. Pronin, Interband optical conductivity of the [001]-oriented Dirac semimetal  $\text{Cd}_3\text{As}_2$ , *Phys. Rev. B* **93**, 121202(R) (2016).
- [39] T. Oka and H. Aoki, All optical measurement proposed for the photovoltaic Hall effect, *J. Phys.* **334**, 012060 (2011).
- [40] D. Yudin, O. Eriksson, and M. I. Katsnelson, Dynamics of quasiparticles in graphene under intense circularly polarized light, *Phys. Rev. B* **91**, 075419 (2015).
- [41] J.-P. Foing, D. Hulin, M. Joffre, M. K. Jackson, J.-L. Oudar, C. Tanguy, and M. Combescot, Absorption Edge Singularities in Highly Excited Semiconductors, *Phys. Rev. Lett.* **68**, 110 (1992).
- [42] C. Tanguy and M. Combescot, X-Ray-Like Singularities for Nonequilibrium Fermi Sea, *Phys. Rev. Lett.* **68**, 1935 (1992).
- [43] A. Pertsova and A. V. Balatsky, Dynamically induced excitonic instability in pumped Dirac materials, *Ann. Phys. (Berlin)* **532**, 1900549 (2020).
- [44] L. V. Hau, S. E. Harris, Z. Dutton, and C. H. Behroozi, Light speed reduction to 17 metres per second in an ultracold atomic gas, *Nature (London)* **397**, 594 (1999).
- [45] C. Liu, Z. Dutton, C. H. Behroozi, and L. V. Hau, Observation of coherent optical information storage in an atomic medium using halted light pulses, *Nature (London)* **409**, 490 (2001).
- [46] A. V. Turukhin, V. S. Sudarshanam, M. S. Shahriar, J. A. Musser, B. S. Ham, and P. R. Hemmer, Observation of Ultraslow and Stored Light Pulses in a Solid, *Phys. Rev. Lett.* **88**, 023602 (2001).
- [47] M. S. Bigelow, N. N. Lepeshkin, and R. W. Boyd, Observation of Ultraslow Light Propagation in a Ruby Crystal at Room Temperature, *Phys. Rev. Lett.* **90**, 113903 (2003).
- [48] M. S. Bigelow, N. N. Lepeshkin, and R. W. Boyd, Superluminal and Slow Light Propagation in a Room-Temperature Solid, *Science* **301**, 200 (2003).
- [49] M. Fleischhauer, A. Imamoglu, and J. P. Marangos, Electromagnetically induced transparency: Optics in coherent media, *Rev. Mod. Phys.* **77**, 633 (2005).
- [50] T. Baba, Slow light in photonic crystals, *Nat. Photonics* **2**, 465 (2008).
- [51] T. V. Trevisan, P. V. Arribi, O. Heinonen, R.-J. Slager, and P. P. Orth, Bicircular Light Floquet Engineering of Magnetic Symmetry and Topology and Its Application to the Dirac Semimetal  $\text{Cd}_3\text{As}_2$ , *Phys. Rev. Lett.* **128**, 066602 (2022).
- [52] H. Dehghani and A. Mitra, Optical Hall conductivity of a Floquet topological insulator, *Phys. Rev. B* **92**, 165111 (2015).